Hyperspectral Unmixing Based on Local Collaborative Sparse Regression

Shaoquan Zhang, Jun Li, *Member, IEEE*, Kai Liu, Chengzhi Deng, Lin Liu, and Antonio Plaza, *Fellow, IEEE*

***Abstract*—Spectral unmixing is an important technique for hyperspectral data exploitation. In order to solve the unmixing problem using a collection of previously available spectral signatures (i.e., a spectral library), sparse unmixing aims at finding the optimal subset of endmembers to represent the pixels in a hyperspectral image. The classic collaborative unmixing globally assumes that all pixels in a hyperspectral scene share the same active set of endmembers. This assumption rarely holds in practice, as endmembers tend to appear localized in spatially homogeneous areas rather than spread over the whole image. To address this limitation, in this letter, we introduce a new strategy to preserve local collaborativity for sparse hyperspectral unmixing. The proposed approach, which is called local collaborative sparse unmixing, considers the fact that endmember signatures generally appear distributed in local spatial regions instead of uniformly distributed throughout the scene. The proposed approach, which includes spatial information in the standard collaborative formulation, has been experimentally validated using both simulated and real hyperspectral data sets.**

***Index Terms*—Hyperspectral imaging, local collaborative sparse regression, sparse unmixing, spectral unmixing.**

I. Introduction

PIXELS in remotely sensed hyperspectral images are likely to be formed by a mixture of pure spectral constituents (*endmembers*), rather than a single substance [1]. Two kinds of spectral unmixing models have been commonly used in the literature to address the mixed pixel problem: linear and nonlinear [2]. On the one hand, the linear model assumes that the spectral response of a pixel is given by a linear combination of the endmembers present in the pixel (see [1] for a detailed description of available techniques for linear unmixing). On the other hand, the nonlinear mixture model assumes that the incident radiation interacts with more than one component and is affected by multiple scattering effects [1]. As a result, nonlinear unmixing generally requires prior knowledge about object geometry and the physical properties of the observed objects [3]. The linear mixture model exhibits practical advantages, such as ease of implementation and flexibility in different applications. In this letter, we will focus exclusively on the linear mixture model.

Techniques based on extracting the endmembers directly from the scene have faced difficulties related with the unavailability of pure signatures in the image data. To overcome this limitation, sparse unmixing [3] has been developed as a semisupervised approach, in which mixed pixels are expressed in the form of linear combinations of a number of pure spectral signatures from a large spectral library that is known in advance [1]. The sparse unmixing algorithm via variable splitting and augmented Lagrangian (SUnSAL) [3] was one of the first methods developed for this purpose, which generally assumes that the number of endmembers participating in each pixel is low. The collaborative SUnSAL (CLSUnSAL) [4] was developed under the assumption that all pixels in a hyperspectral image share the same active set of endmembers. This global assumption rarely holds in practice, as endmembers typically appear localized in spatially homogeneous regions instead of uniformly distributed through the scene [5], [6].

Previous works have explored the possibility of including spatial information in the analysis of hyperspectral data [7]–[11]. For instance, several local unmixing methods based on image endmember extraction have been developed [12]–[14], which make full use of the spatial information. On the other hand, some methods aim at exploiting spatial–contextual information under the sparse regression framework (see, for example, [15] and [16]). SUnSAL-TV [15] includes a total variation (TV) regularizer to promote spatial homogeneity among neighboring pixels. However, SUnSAL-TV may lead to oversmoothness and blurred boundaries. Other works aimed at exploiting the spatial–contextual information in the sparse model [17]–[19] have shown that the local spatial information plays an important role in sparse unmixing as unmixing problems generally become easier in a local scale rather than a global scale.

Based on the observation that local information can promote sparse representation while collaborativity can avoid overestimation of the number of endmembers and their abundances, in this letter, we introduce a new strategy to preserve local collaborativity for sparse hyperspectral unmixing. The proposed approach, which is called local collaborative sparse unmixing (LCSU), assumes that neighboring pixels share the same active set of endmembers. In comparison with the global assumption enforced by CLSUnSAL, the proposed LCSU assumes that

Manuscript received September 30, 2015; revised December 30, 2015; accepted January 21, 2016. Date of publication March 14, 2016; date of current version April 20, 2016. This work was supported by the Jiangxi Science and Technology Research Project of Education Department of China under Grant GJJ14764.

S. Zhang, J. Li, and K. Liu are with the Center of Integrated Geographic Information Analysis and Guangdong Provincial Key Laboratory of Urbanization and Geo-simulation, School of Geography and Planning, Sun Yat-sen University, Guangzhou 510275, China (e-mail: liuk6@mail.sysu.edu.cn).

C. Deng is with the Department of Information Engineering, Nanchang Institute of Technology, Nanchang 330099, China.

L. Liu is with the Center of Integrated Geographic Information Analysis and Guangdong Provincial Key Laboratory of Urbanization and Geo-simulation, School of Geography and Planning, Sun Yat-sen University, Guangzhou 510275, China, and also with the Department of Geography, University of Cincinnati, Cincinnati, OH 45221 USA.

A. Plaza is with the Hyperspectral Computing Laboratory, Department of Technology of Computers and Communications, Escuela Politécnica, University of Extremadura, 10071 Cáceres, Spain.

Color versions of one or more of the figures in this paper are available online at http://ieeexplore.ieee.org.

Digital Object Identifier 10.1109/LGRS.2016.2527782

endmembers tend to appear localized in spatially homogeneous areas instead of distributed over the full image. The proposed approach can also preserve global collaborativity (e.g., in the case that an endmember appears in the whole image), since it generalizes to global collaborativity through local searching.

II. Collaborative Sparse Unmixing

Sparse unmixing finds a linear combination of endmembers for an observed pixel i from a large spectral library as follows:

$$\mathbf{y}_i = \mathbf{A}\mathbf{x}_i + \mathbf{n}_i \tag{1}$$

where $\mathbf{y}_i$ denotes an $L \times 1$ pixel vector of the observed hyperspectral data, L denotes the number of bands, $\mathbf{A} \in \mathbb{R}^{L\times m}$ is a spectral library, m is the number of spectral signatures in $\mathbf{A}$, $\mathbf{x}_i$ denotes the abundance vector corresponding to library $\mathbf{A}$, and $\mathbf{n}_i$ is an $L \times 1$ vector collecting the errors affecting the measurements at each spectral band. As the number of endmembers involved in a mixed pixel is usually very small when compared with the size of the spectral library, the vector of fractional abundances $\mathbf{x}$ is sparse [20]. The unmixing problem can be formulated as an $\ell_2 - \ell_0$ norm optimization problem

$$\min_{\mathbf{x}_i} \ \frac{1}{2}\|\mathbf{A}\mathbf{x}_i - \mathbf{y}_i\|_2^2 + \lambda\|\mathbf{x}_i\|_0 \ \text{ s.t. } \mathbf{x}_i \geq 0 \tag{2}$$

where $\|\mathbf{x}_i\|_0$ denotes the number of the nonzero components of the vector $\mathbf{x}_i$, and λ is a regularization parameter that weights the two terms of the objective function. However, the ℓ_0 term leads to an NP-hard problem, and thus, it is very difficult to solve. In [21] and [22], it was proven that the ℓ_0 norm can be replaced by the ℓ_1 norm under a certain condition of the restricted isometric property. In this context, the previous problem becomes

$$\min_{\mathbf{x}_i} \ \frac{1}{2}\|\mathbf{A}\mathbf{x}_i - \mathbf{y}_i\|_2^2 + \lambda\|\mathbf{x}_i\|_1 \ \text{ s.t. } \mathbf{x}_i \geq 0 \tag{3}$$

where $\|\mathbf{x}_i\|_1 = \sum_{j=1}^{m} |x_j|$ denotes the ℓ_1 norm, x_j is the jth value of $\mathbf{x}_i$, and the optimization problem in (3) is convex. Despite its wide use for solving unmixing, the solution to this problem is highly influenced by the high mutual coherence of the libraries [1]. In [4], an $\ell_{2,1}$ mixed norm (called collaborative regularization) was proposed, which globally imposes sparsity among the endmembers in collaborative fashion for all pixels. Let $\mathbf{X} = [\mathbf{x}_1, \mathbf{x}_2, \ldots, \mathbf{x}_n]$ be the abundance fractions that correspond to the sparse solution, where n is the number of pixels in the image. Collaborative sparse regression can be formulated as follows:

$$\min_{\mathbf{X}} \frac{1}{2}\|\mathbf{A}\mathbf{X} - \mathbf{Y}\|_F^2 + \lambda \sum_{k=1}^{m} \|\mathbf{x}^k\|_2 \ \text{ s.t. } \mathbf{X} \geq 0 \tag{4}$$

where $\mathbf{x}^k$ denotes the kth line of matrix $\mathbf{X}$ $(k = 1, 2, \ldots, m)$, and $\sum_{k=1}^{m} \|\mathbf{x}^k\|_2$ is the so-called $\ell_{2,1}$ mixed norm. Notice that the main difference between SUnSAL and CLSUnSAL is that the former employs pixelwise independent regressions, whereas the latter enforces joint sparsity among all the pixels. That is, as shown in (4), the collaborative sparse regression globally assumes that all the pixels share the same active set of endmembers. More recently, SUnSAL-TV incorporated spatial–contextual relationships into the sparse unmixing model [15]. SUnSAL-TV promotes piecewise-smooth transitions in the fractional abundance of the same endmember among the first-order neighborhood pixels, as shown in the following:

$$\min_{\mathbf{X}} \ \frac{1}{2}\|\mathbf{A}\mathbf{X} - \mathbf{Y}\|_F^2 + \lambda\|\mathbf{X}\|_{1,1} + \lambda_{\text{TV}}\text{TV}(\mathbf{X})$$
$$\text{s.t.} \quad \mathbf{X} \geq 0 \tag{5}$$

where $\text{TV}(\mathbf{X}) \equiv \sum_{i,j\in\varepsilon} \|\mathbf{x}_i - \mathbf{x}_j\|_1$, ε represents the set of (horizontal and vertical) pixel neighbors in the image.

III. LCSU

Here, a new sparse unmixing method is proposed that introduces a local collaborative assumption. LCSU assumes that the neighboring pixels share the same active set of endmembers as follows:

$$\min_{\mathbf{x}} \frac{1}{2}\|\mathbf{A}\mathbf{X} - \mathbf{Y}\|_F^2 + \lambda \sum_{i=1}^{n}\sum_{k=1}^{m} \left\|\mathbf{x}^k_{j\in\mathcal{N}(i)}\right\|_2$$
$$\text{s.t. } \mathbf{x} \geq 0 \tag{6}$$

where $\mathcal{N}(i)$ is the neighborhood of pixel i, and λ is a regularization parameter controlling the degree of sparseness. The main difference between the proposed approach and SUnSAL-TV is that LCSU imposes collaborative sparsity among neighboring pixels, whereas SUnSAL-TV aims at promoting piecewise-smooth transitions in abundance estimations. In other words, SUnSAL-TV enforces that neighboring pixels share similar fractional abundances for the same endmember, whereas LCSU focuses on imposing local collaborativity among the full set of endmembers, thus addressing problems observed in SUnSAL-TV such as oversmoothed or blurred abundance maps. The main difference between problem (6) and problem (4) is that LCSU introduces spatial information to promote *local* collaborativity, whereas CLSUnSAL focuses on *global* collaborativity. In comparison with CLSUnSAL, the proposed LCSU assumes that neighboring pixels share the same support. This is more realistic, as a given endmember is likely to appear localized in a spatially homogeneous region rather than in the whole image. As shown in (6), the first term accounts for the pixel reconstruction error, whereas the second term imposes sparsity in the solution. We use the variable splitting and the augmented Lagrangian method in [23] to solve the $\ell_2 + \ell_{2,1}$ norm optimization problem (6), as described in the following.

Following [3], let $\mathcal{L}(\mathbf{U}, \mathbf{V}, \mathbf{D}) \equiv g(\mathbf{U}, \mathbf{V}) + (\mu/2)\|\mathbf{G}\mathbf{U} - \mathbf{B}\mathbf{V} - \mathbf{D}\|_F^2$ be the augmented Lagrangian for

$$\min_{\mathbf{U},\mathbf{V}} g(\mathbf{V}) \ \text{ subject to } \mathbf{G}\mathbf{U} + \mathbf{B}\mathbf{V} = 0$$

where $\mu > 0$ is a positive constant, and $\mathbf{D}/\mu$ denotes the Lagrange multipliers associated to the constraint $\mathbf{G}\mathbf{U} + \mathbf{B}\mathbf{V} = 0$; $\mathbf{V} \equiv (\mathbf{V}_1, \mathbf{V}_2, \mathbf{V}_3)$, $\mathbf{G} = [\mathbf{A}, \mathbf{I}, \mathbf{I}]^T$, $\mathbf{B} = \text{diag}(-\mathbf{I})$; $g(\mathbf{V}) \equiv (1/2)\|\mathbf{V}_1 - \mathbf{Y}\|_F^2 + \lambda\|\mathbf{V}_2\| + \iota_{R+}(\mathbf{V}_3)$ is the cost function of the following optimization problem:

$$\min_{\mathbf{U},\mathbf{V}_1,\mathbf{V}_2,\mathbf{V}_3} \ \frac{1}{2}\|\mathbf{V}_1 - \mathbf{Y}\|_F^2 + \lambda\|\mathbf{V}_2\|_2 + \iota_{R+}(\mathbf{V}_3)$$
$$\text{s.t.} \qquad \mathbf{V}_1 = \mathbf{A}\mathbf{U}, \mathbf{V}_2 = \mathbf{U}, \mathbf{V}_3 = \mathbf{U} \tag{7}$$

where $\iota_{R+}(\mathbf{X}) = \sum_{i=1}^{n} \iota_{R+}(\mathbf{x}_i)$ is the indicator function, and $\iota_{R+}(\mathbf{x}_i)$ is zero if $\mathbf{x}_i$ belongs to the nonnegative orthant and

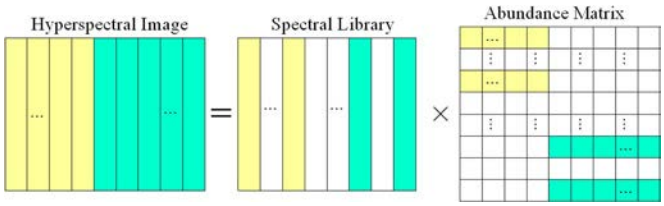

Fig. 1. Graphical illustration of the proposed local collaborative regularizer. Active members of the spectral library are highlighted in yellow and green color (different colors represent different regions), whereas nonactive members are highlighted in white color. Instead of promoting full active lines in the estimated abundance matrix, LCSU promotes discontinuous lines related with neighboring pixels that share locally active endmembers.

$+\infty$ otherwise. Problem (7) is equivalent to the optimization problem (6) via the adaptation, by setting $\mathbf{U} = \mathbf{X}$, as follows:

$$\min_{\mathbf{x}} \frac{1}{2}\|\mathbf{AX} - \mathbf{Y}\|_F^2 + \lambda \sum_{i=1}^{n} \sum_{k=1}^{m} \left\| \mathbf{x}^k_{j \in \mathcal{N}(i)} \right\|_2 + \iota_{R+}(\mathbf{X}).$$

Now, we can implement the alternative direction method of multipliers [24] to solve the optimization problem involved in LCSU, as shown in Algorithm 1.

Algorithm 1 Pseudocode of the LCSU Algorithm

1: **Initialization**:
2: set $k = 0$, choose $\mu \geq 0, \mathbf{U}^{(0)}, \mathbf{V}_1^{(0)}, \mathbf{V}_2^{(0)}, \mathbf{V}_3^{(0)}, \mathbf{D}^{(0)}$
3: **Repeat**:
4: $\mathbf{U}^{(k+1)} \leftarrow \arg\min_{\mathbf{U}} \mathcal{L}(\mathbf{U}, \mathbf{V}_1^{(k)}, \mathbf{V}_2^{(k)}, \mathbf{V}_3^{(k)}, \mathbf{D}^{(k)})$
5: $\mathbf{V}_1^{(k+1)} \leftarrow \arg\min_{\mathbf{V}_1} \mathcal{L}(\mathbf{U}^{(k+1)}, \mathbf{V}_1, \mathbf{V}_2^{(k)}, \mathbf{V}_3^{(k)})$
6: $\mathbf{V}_2^{(k+1)} \leftarrow \arg\min_{\mathbf{V}_2} \mathcal{L}(\mathbf{U}^{(k+1)}, \mathbf{V}_1^{(k)}, \mathbf{V}_2, \mathbf{V}_3^{(k)})$
7: $\mathbf{V}_3^{(k+1)} \leftarrow \arg\min_{\mathbf{V}_3} \mathcal{L}(\mathbf{U}^{(k+1)}, \mathbf{V}_1^{(k)}, \mathbf{V}_2^{(k)}, \mathbf{V}_3)$
8: **Update Lagrange multipliers**:
9: $\mathbf{D}^{(k+1)} \leftarrow \mathbf{D}^{(k)} - \mathbf{AU}^{(k+1)} + \mathbf{V}^{(k+1)}$
9: **Update iteration**: $k \leftarrow k + 1$
10: **until** the stopping criterion is satisfied.

For illustrative purposes, Fig. 1 graphically illustrates the performance of the local collaborative regularizer. The endmembers highlighted in yellow color are assumed to be only active in the yellow region, whereas the endmembers in green color are only active in the green region. Nonactive members are highlighted in white color. If endmembers appear active in every pixel, we would have a few fully active lines in the estimated abundance matrix. Instead, the LCSU promotes discontinuous lines in the estimated abundance matrix, which are related with neighboring pixels that share locally active endmembers.

IV. Experiments With Simulated Data

Here, two simulated data sets were used to evaluate the performance of the proposed algorithm in comparison to SUnSAL [3], CLSUnSAL [4], and SUnSAL-TV [15]. It should be noted that we use four connected neighborhoods for methods that involve local information. The signal-to-reconstruction error (SRE) is used to evaluate the unmixing accuracy. Let $\widehat{\mathbf{x}}_i$ be the estimated abundance of $\mathbf{x}_i$, and let $\mathbf{x}_i$ be the true abundance.

TABLE I
SRE Values (Along With Their Standard Deviation) and p_s (in Brackets) Achieved After Applying Different Unmixing Methods to the Considered Simulated Data Set With Different SNR Values. The Optimal Parameters for Which the Reported Values Were Achieved Are Indicated in the Parentheses

SNR(dB)	SUnSAL	CLSUnSAL	SUnSAL-TV	LCSU
30	5.19±0.03 (0.57) $\lambda = 3e\text{-}2$	7.53±0.03 (0.88) $\lambda = 1e\text{-}1$	8.04±0.04 (0.90) $\lambda = 1e\text{-}5$; $\lambda_{TV} = 3e\text{-}3$	8.13±0.05 (0.90) $\lambda = 5e\text{-}3$
40	8.52±0.05 (0.82) $\lambda = 1e\text{-}4$	9.27±0.02 (0.89) $\lambda = 7e\text{-}3$	10.41±0.01 (0.90) $\lambda = 1e\text{-}5$; $\lambda_{TV} = 5e\text{-}4$	10.57±0.01 (0.90) $\lambda = 4e\text{-}3$
50	15.03±0.14 (0.99) $\lambda = 2e\text{-}5$	15.63±0.13 (1.00) $\lambda = 2e\text{-}4$	16.35±0.19 (1.00) $\lambda = 2e\text{-}5$; $\lambda_{TV} = 5e\text{-}6$	18.30±0.17 (1.00) $\lambda = 8e\text{-}5$

The SRE can be computed as follows:

$$\text{SRE}(\mathbf{x}_i) = 10 \cdot \log_{10} \left(\frac{E\left(\|\mathbf{x}_i\|_2^2\right)}{E\left(\|\mathbf{x}_i - \widehat{\mathbf{x}}_i\|_2^2\right)} \right) \tag{8}$$

where $E(\cdot)$ denotes the expectation function. The larger the SRE, the more accurate the unmixing. Furthermore, we use another indicator, i.e., the "probability of success," $p_s \equiv P(\|\widehat{\mathbf{x}}_i - \mathbf{x}_i\|^2/\|\mathbf{x}_i\|^2 \leq \text{threshold})$, which is an estimate of the probability that the relative error power be smaller than a certain threshold [3]. In our case, the estimation result is considered successful when $\|\widehat{\mathbf{x}}_i - \mathbf{x}_i\|^2/\|\mathbf{x}_i\|^2 \leq 3.16$ (5 dB); this threshold was demonstrated in previous work to provide satisfactory results [3]. In our experiments, the spectral library $\mathbf{A}$ is a dictionary of minerals extracted from the U.S. Geological Survey (USGS) library [25]. The library $\mathbf{A}$ contains $m = 240$ materials with $L = 224$ bands. For all the tested algorithms, the input parameters have been carefully tuned for optimal performance, and all reported results correspond to the average of 15 algorithm executions.

A. Simulated Experiment 1

The first synthetic data set has been simulated with four different regions (a total of $n = 1600$ pixels) with three spectral signatures for each region selected from the library $\mathbf{A}$. The fractional abundances of the endmembers follow a Dirichlet distribution [26]. Gaussian noise is added to the simulated scene with different levels of the signal-to-noise ratio (SNR $= 30, 40$, and 50 dB). Table I shows the SRE (in decibels) results along with the standard deviation and p_s achieved by the considered algorithms. Notice that, for SUnSAL-TV, the results are obtained by using a nonisotropic type of TV, which are better than those obtained from the isotropic version. Several conclusions can be obtained in Table I. First and foremost, the proposed LCSU obtains the best results in all cases. This is because LCSU can preserve local collaborativity in this particular case. Furthermore, both SUnSAL-TV and LCSU (which include spatial information) outperform SUnSAL and CLSUnSAL. This is expected, as local regions are likely to share similar active supports. Finally, LCSU and CLSUnSAL exhibit better performance in comparison with SUnSAL. This is consistent with [4].

In order to evaluate the computational cost of the proposed LCSU, Table II reports the processing times for the case of SNR $= 40$ dB in Table I. All the algorithms were implemented using MATLAB R2012a on a desktop computer equipped with an Intel Core 5 Duo central processing unit (at 3.2 GHz) and 4 GB of RAM memory. It can be observed that, in the case

TABLE II
TIME IN SECONDS TO PROCESS THE FIRST SIMULATED DATA SET

Algorithm	SUnSAL	CLSUnSAL	SUnSAL-TV	LCSU
Time(s)	8.8789	26.1904	123.5209	48.4201

TABLE III
SRE VALUES (ALONG WITH THEIR STANDARD DEVIATION) AND p_s (IN BRACKETS) ACHIEVED AFTER APPLYING DIFFERENT UNMIXING METHODS TO THE SECOND SIMULATED DATA SET. THE OPTIMAL PARAMETERS ARE REPORTED

SNR	SUnSAL	CLSUnSAL	SUnSAL-TV	LCSU
30	4.02±0.01 (0.52) $\lambda = 6e\text{-}3$	4.39±0.02 (0.56) $\lambda = 5e\text{-}3$	5.41±0.02 (0.64) $\lambda = 1e\text{-}4$; $\lambda_{TV} = 3e\text{-}3$	5.51±0.03 (0.64) $\lambda = 6e\text{-}3$
40	8.93±0.02 (0.83) $\lambda = 5e\text{-}4$	9.97±0.05 (0.86) $\lambda = 9e\text{-}4$	11.31±0.02 (0.95) $\lambda = 1e\text{-}4$; $\lambda_{TV} = 4e\text{-}4$	11.90±0.02 (0.96) $\lambda = 1e\text{-}3$
50	16.54±0.06 (1.00) $\lambda = 1e\text{-}4$	17.00±0.07 (1.00) $\lambda = 2e\text{-}3$	18.47±0.07 (1.00) $\lambda = 1e\text{-}4$; $\lambda_{TV} = 6e\text{-}5$	18.93±0.05 (1.00) $\lambda = 6e\text{-}4$

that spatial information is included, LCSU is much faster than SUnSAL-TV, whereas both algorithms are slower than SUnSAL and CLSUnSAL due to the increased model complexity.

B. Simulated Experiment 2

In a second experiment, we consider a more complicated and realistic problem. The fractional abundances used in the simulation follow a Dirichlet distribution uniformly over the probability simplex. In order to evaluate the impact of using a larger dictionary, a new library with $m = 342$ materials and $L = 224$ bands is considered. Nine signatures are randomly chosen from the library, and a 100×100 pixel data cube of true observations is generated. The fractional abundances are piecewise smooth, i.e., they exhibit smooth abundance value transitions among neighboring pixels (see a detailed description about simulated data cube 2 in [15]). These data exhibit spatial homogeneity, thus allowing us to study the impact of including spatial information in the considered unmixing algorithms. Noise with different SNR values has been included in experiments, and we studied the consistency of the results across different runs and random generations of the data sets. Table III shows the SRE (in decibels) values, along with their standard deviation, and p_s achieved by the different tested algorithms under different SNR values. In Table III, we can conclude that LCSU exhibits competitive results in comparison with the other algorithms. This is expected, as LCSU preserves local information, as compared with CLSUnSAL, and enforces collaborativity as opposed to SUnSAL-TV.

V. EXPERIMENTAL RESULTS WITH REAL DATA

In our real data experiments, we use the well-known Airborne Visible Infrared Imaging Spectrometer (AVIRIS) Cuprite data set, available online in reflectance units (http://aviris.jpl.nasa.gov/html/aviris.freedata.html). The portion used in experiments corresponds to a 250×191 pixel subset of the scene, with 224 spectral bands in the range of 0.4–2.5 μm and the nominal spectral resolution of 10 nm. Prior to the analysis, bands 1–2, 105–115, 150–170, and 223–224 were removed due to water absorption and low SNR, leaving a total of 188 spectral bands. The spectral library used in this experiment is the same library $\mathbf{A}$ used in our simulated experiments, and the noisy bands are also removed from $\mathbf{A}$. For illustrative purposes,

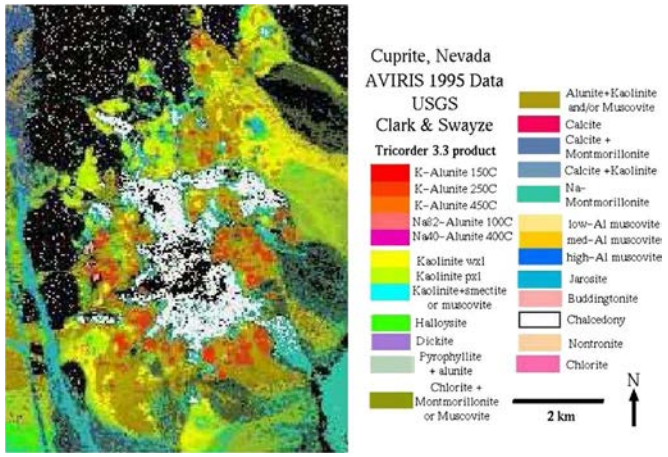

Fig. 2. USGS map showing the location of different minerals in the Cuprite mining district in Nevada.

Fig. 2 shows a mineral map produced in 1995 by USGS, in which the Tricorder 3.3 software product [27] was used to map different minerals present in the Cuprite mining district. The USGS map serves as a good indicator for qualitative assessment of the fractional abundance maps produced by the different unmixing algorithms.

Fig. 3 conducts a qualitative comparison between the classification maps produced by the USGS Tricorder algorithm and the fractional abundances estimated by SUnSAL, CLSUnSAL, SUnSAL-TV, and LCSU algorithms for three highly representative minerals in the Cuprite mining district (alunite, buddingtonite, and chalcedony). In this experiment, the regularization parameters used for SUnSAL, CLSUnSAL, and LCSU were empirically set to $\lambda = 0.001$, 0.01, and 0.01, respectively, whereas the ones corresponding to SUnSAL-TV were set to $\lambda = 0.0005$, $\lambda_{\mathrm{TV}} = 0.005$. As shown in Fig. 3, all results obtained by the four considered unmixing methods show a good correlation of the features present in the estimated abundance maps, with respect to the classification maps produced by the USGS Tricorder algorithm. The average numbers of endmembers with abundances higher than 0.05 estimated by LCSU, SUnSAL-TV, CLSUnSAL, and SUnSAL are 2.438, 2.415, 2.297, and 2.098, respectively (per pixel). These small differences lead to the conclusion that LCSU uses a smaller number of endmembers to explain the data, thus enforcing sparsity. Although a quantitative evaluation of the obtained results is very difficult with real data, we can qualitatively observe that some of the LCSU-derived abundance maps (e.g., Chalcedony mineral) present less blurring and oversmoothness than those produced by SUnSAL-TV. Thus, we can qualitatively conclude that LCSU is a valid tool for including spatial information in sparse unmixing of real hyperspectral data.

VI. CONCLUSION

In this letter, we have developed a new local collaborative method for sparse unmixing of hyperspectral data. The proposed approach adopts a local assumption by means of which spatially neighboring pixels share similar active sets of endmembers. Our experiments with both simulated and real hyperspectral data reveal that the LCSU algorithm consistently achieves good spectral unmixing performance in comparison with other state-of-the-art approaches.

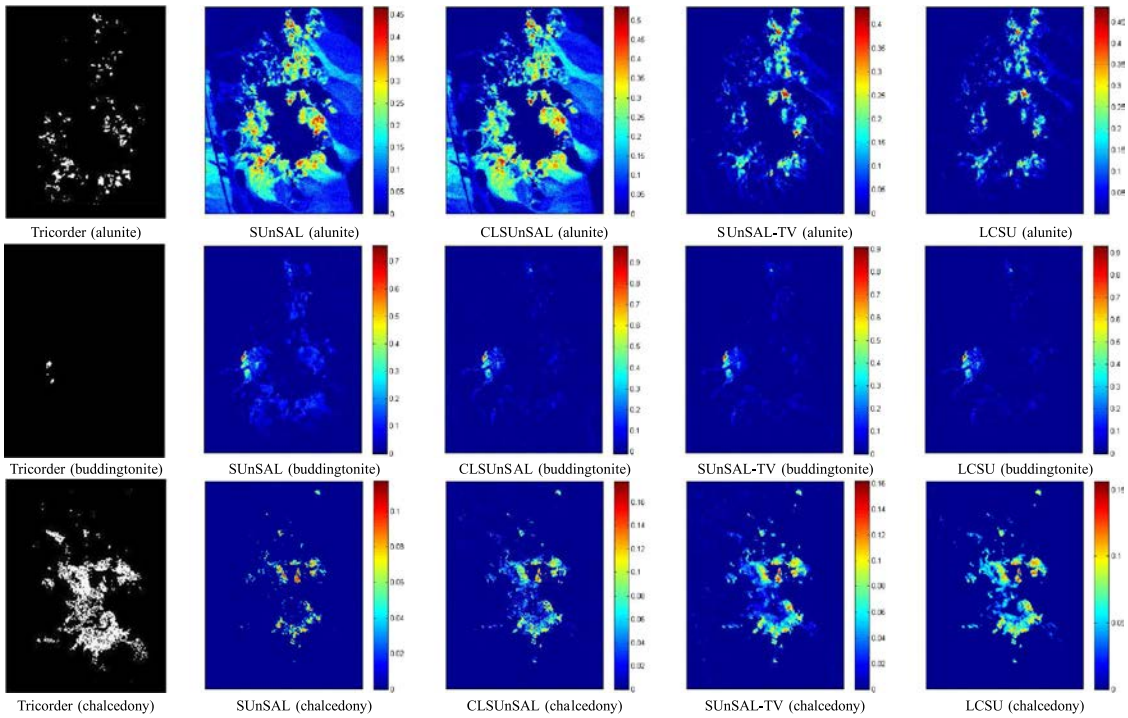

Fig. 3. Fractional abundance maps estimated by SUnSAL, CLSUnSAL, SUnSAL-TV, and LCSU, as compared with the classification maps produced by USGS Tricorder software for the considered 250 × 191 pixel subset of the AVIRIS Cuprite scene.

REFERENCES

[1] J. Bioucas-Dias *et al.*, "Hyperspectral unmixing overview: Geometrical, statistical, and sparse regression-based approaches," *IEEE J. Sel. Topics Appl. Earth Observ. Remote Sens.*, vol. 5, no. 2, pp. 354–379, Apr. 2012.

[2] N. Keshava and J. Mustard, "Spectral unmixing," *IEEE Signal Process. Mag.*, vol. 19, no. 1, pp. 44–57, Jan. 2002.

[3] M.-D. Iordache, J. Bioucas-Dias, and A. Plaza, "Sparse unmixing of hyperspectral data," *IEEE Trans. Geosci. Remote Sens.*, vol. 49, no. 6, pp. 2014–2039, Jun. 2011.

[4] M.-D. Iordache, J. Bioucas-Dias, and A. Plaza, "Collaborative sparse regression for hyperspectral unmixing," *IEEE Trans. Geosci. Remote Sens.*, vol. 52, no. 1, pp. 341–354, Jan. 2014.

[5] G. Martin and A. Plaza, "Spatial-spectral preprocessing prior to endmember identification and unmixing of remotely sensed hyperspectral data," *IEEE J. Sel. Topics Appl. Earth Observ. Remote Sens.*, vol. 5, no. 2, pp. 380–395, Apr. 2012.

[6] G. Martin and A. Plaza, "Region-based spatial preprocessing for endmember extraction and spectral unmixing," *IEEE Geosci. Remote Sens. Lett.*, vol. 8, no. 4, pp. 745–749, Jul. 2011.

[7] Y. Chen, N. Nasrabadi, and T. Tran, "Hyperspectral image classification via kernel sparse representation," *IEEE Trans. Geosci. Remote Sens.*, vol. 51, no. 1, pp. 217–231, Jan. 2013.

[8] T. Lu, S. Li, L. Fang, Y. Ma, and J. Benediktsson, "Spectral-spatial adaptive sparse representation for hyperspectral image denoising," *IEEE Trans. Geosci. Remote Sens.*, vol. 54, no. 1, pp. 373–385, Jan. 2016.

[9] S. Mei, M. He, Z. Wang, and D. Feng, "Spatial purity based endmember extraction for spectral mixture analysis," *IEEE Trans. Geosci. Remote Sens.*, vol. 48, no. 9, pp. 3434–3445, Sep. 2010.

[10] O. Eches, N. Dobigeon, and J. Y. Tourneret, "Enhancing hyperspectral image unmixing with spatial correlations," *IEEE Trans. Geosci. Remote Sens.*, vol. 49, no. 11, pp. 4239–4247, Nov. 2011.

[11] M. Xu, L. Zhang, and B. Du, "An image-based endmember bundle extraction algorithm using both spatial and spectral information," *IEEE J. Sel. Topics Appl. Earth Observ. Remote Sens.*, vol. 8, no. 6, pp. 2607–2617, Jun. 2015.

[12] K. Canham, A. Schlamm, A. Ziemann, B. Basener, and D. Messinger, "Spatially adaptive hyperspectral unmixing," *IEEE Trans. Geosci. Remote Sens.*, vol. 49, no. 11, pp. 4248–4262, Nov. 2011.

[13] M. Goenaga, M. Torres-Madronero, M. Velez-Reyes, S. Van Bloem, and J. Chinea, "Unmixing analysis of a time series of Hyperion images over the Guanica Dry Forest in Puerto Rico," *IEEE J. Sel. Topics Appl. Earth Observ. Remote Sens.*, vol. 6, no. 2, pp. 329–338, Apr. 2013.

[14] A. Zare and P. Gader, "Piece-wise convex spatial-spectral unmixing of hyperspectral imagery using possibilistic and fuzzy clustering," in *Proc. IEEE Int. Conf. FUZZ*, Jun. 2011, pp. 741–746.

[15] M.-D. Iordache, J. Bioucas-Dias, and A. Plaza, "Total variation spatial regularization for sparse hyperspectral unmixing," *IEEE Trans. Geosci. Remote Sens.*, vol. 50, no. 11, pp. 4484–4502, Nov. 2012.

[16] X. Zhao, F. Wang, T. Huang, M. Ng, and R. Plemmons, "Deblurring and sparse unmixing for hyperspectral images," *IEEE Trans. Geosci. Remote Sens.*, vol. 51, no. 7, pp. 4045–4058, Jul. 2013.

[17] Z. Lai, Y. Li, M. Wan, and Z. Jin, "Local sparse representation projections for face recognition," *Neural Comput. Appl.*, vol. 23, no. 7/8, pp. 2231–2239, Dec. 2013.

[18] L. Yue, H. Shen, Q. Yuan, and L. Zhang, "A locally adaptive l_1-l_2 norm for multi-frame super resolution of images with mixed noise and outliers," *Signal Process.*, vol. 105, no. 9, pp. 156–174, Dec. 2014.

[19] M. Veganzones, G. Tochon, M. Dalla-Mura, A. Plaza, and J. Chanussot, "Hyperspectral image segmentation using a new spectral unmixing-based binary partition tree representation," *IEEE Trans. Image Process.*, vol. 23, no. 8, pp. 3574–3589, Aug. 2014.

[20] Z. Shi, W. Tang, Z. Duren, and Z. Jiang, "Subspace matching pursuit for sparse unmixing of hyperspectral data," *IEEE Trans. Geosci. Remote Sens.*, vol. 52, no. 6, pp. 3256–3274, Jun. 2014.

[21] E. Candès and T. Tao, "Decoding by linear programming," *IEEE Trans. Inf. Theory*, vol. 51, no. 12, pp. 4203–4215, Dec. 2005.

[22] E. Candès and T. Tao, "Near-optimal signal recovery from random projections: Universal encoding strategies," *IEEE Trans. Inf. Theory*, vol. 52, no. 12, pp. 5406–5425, Dec. 2006.

[23] M. Afonso, J. Bioucas-Dias, and M. Figueiredo, "An augmented Lagrangian approach to the constrained optimization formulation of imaging inverse problems," *IEEE Trans. Image Process.*, vol. 20, no. 3, pp. 681–695, Mar. 2011.

[24] J. Eckstein and D. Bertsekas, "On the Douglas-Rachford splitting method and the proximal point algorithm for maximal monotone operators," *Math. Programm.*, vol. 55, no. 3, pp. 293–318, Jun. 1992.

[25] R. Clark, G. Swayze, A. Gallagher, T. King, and W. Calvin, "The U.S. geological survey digital spectral library: Version 1: 0.2 to 3.0 microns," U.S. Geological Survey, Denver, CO, USA, pp. 93–592, 1993.

[26] J. Nascimento and J. Bioucas-Dias, "Vertex component analysis: A fast algorithm to unmix hyperspectral data," *IEEE Trans. Geosci. Remote Sens.*, vol. 43, no. 4, pp. 898–910, Apr. 2005.

[27] R. Clark *et al.*, "Imaging spectroscopy: Earth and planetary remote sensing with the USGS Tetracorder and expert systems," *J. Geophys. Res.*, vol. 108, no. E12, pp. 5131–5135, Dec. 2003.